



Published in final edited form as:

J Cogn Neurosci. 2014 June ; 26(6): 1266–1282. doi:10.1162/jocn_a_00538.

Reorganization of Retinotopic Maps After Occipital Lobe Infarction

Lucia M. Vaina^{1,2,3}, Sergei Soloviev³, Finnegan J. Calabro³, Ferdinando Buonanno^{1,2,3}, Richard Passingham⁴, and Alan Cowey^{3,4,5}

¹Massachusetts General Hospital, Department of Neurology, Boston, MA, USA, 02214

²Harvard Medical School, Department of Neurology, Boston, MA, USA, 02215

³Boston University, Departments of Biomedical Engineering and Neuroscience, Boston, MA, USA, 02215

⁴University of Oxford, Department of Experimental Psychology, Oxford OX1 3UD, UK

Abstract

We studied patient JS who had a right occipital infarct that encroached on visual areas V1, V2v and VP. When tested psychophysically, he was very impaired at detecting the direction of motion in random dot displays where a variable proportion of dots moving in one direction (signal) were embedded in masking motion noise (noise dots). The impairment on this Motion Coherence task was especially marked when the display was presented to the upper left (affected) visual quadrant, contralateral to his lesion. However, with extensive training, by 11 months his threshold fell to the level of healthy subjects. Training on the Motion Coherence task generalized to another motion task, the Motion Discontinuity task, on which he had to detect the presence of an edge that was defined by the difference in the direction of the coherently moving dots (signal) within the display. He was much better at this task at 8 than 3 months, and this improvement was associated with an increase in the activation of the human MT complex (hMT+) and in the kinetic occipital region (KO) as shown by repeated fMRI scans.

We also used fMRI to perform retinotopic mapping at 3, 8 and 11 months after the infarct. We quantified the retinotopy and areal shifts by measuring the distances between the center of mass of functionally defined areas, computed in spherical surface-based coordinates. The functionally defined retinotopic areas V1, V2v, V2d and VP were initially smaller in the lesioned right hemisphere, but they increased in size between 3 and 11 months. This change was not found in the normal, left hemisphere, of the patient or in either hemispheres of the healthy control subjects.

We were interested in whether practice on the motion coherence task promoted the changes in the retinotopic maps. We compared the results for patient JS with those from another patient (PF) who had a comparable lesion but had not been given such practice. We found similar changes in the maps in the lesioned hemisphere of PF. However, PF was only scanned at 3 and 7 months, and the biggest shifts in patient JS were found between 8 and 11 months. Thus, it is important to carry out

Corresponding author: Lucia M. Vaina: vaina@bu.edu.

⁵Deceased 12. 2012

a prospective study with a trained and untrained group so as to determine whether the patterns of reorganization that we have observed can be further promoted by training.

Introduction

People can recover remarkably well from the effects of cortical lesions. This is best demonstrated in the case of lesions that involve either sensory or motor areas. Physiological techniques can be used to identify and then map the damaged region. The same techniques can then be used to chart whether after the damage there are changes in the mapping over time.

There is an added advantage in working with a sensory system, since sensory thresholds provide an objective measure of improvement. For example, the threshold for discriminating the direction of motion can be measured as the minimum number of dots that have to move coherently for motion to be detected. Vaina et al. (Vaina et al. 2001) showed that if patients with unilateral lesions of the MT complex (hMT+) are tested repeatedly, some could regain normal thresholds, even when the displays are presented to the affected hemisphere. Huxlin et al. (Huxlin et al. 2009) reported that similar recovery could be found after large lesions of V1. Moore et al. (Moore et al. 2001) made striate lesions in monkeys and reported that they could detect the direction of coherent motion so long as the displays were large. However, in this case the lesions were made soon after birth whereas in the study by Huxlin et al. the patients suffered lesions as adults.

One possibility that could explain these results is that improvement can occur because of changes in the sensory maps. These maps have turned out to be surprisingly plastic. We distinguish three situations. For all three there are supporting data from experiments in cats and monkeys.

The first involves changes that occur in primary sensory maps after the peripheral input to part of the map is cut off. For example, remapping can occur in area S1 after the loss of a digit (Merzenich et al. 1984) or section of the dorsal column (Jain et al. 2008), and in V1 after a retinal lesion (Chino 1995). The finding is that, over time, neurons in the deafferented part of the map can become responsive to stimulation of the adjacent tissue. If the lesion is complete, as in the loss of a digit or section of the dorsal column, it is stimulation of the neighboring digit (Merzenich et al. 1984) or face (Jain et al. 2008) that evokes responses. If the lesion is incomplete, as in the case of small retinal lesions, it is stimulation of the retina adjacent to the lesion that does so (Chino 1995).

In these cases, cell activity is weak at first (Chen et al. 2012) and it is not yet clear to what extent it can become normal over time. Chino et al. (Chino 1995) recorded from neurons and claimed that three months after a bilateral retinal lesion the responses were relatively normal so long as the stimuli were high contrast. Smirnakis et al. (Smirnakis et al. 2005) queried this claim, and reported that V1 did not regain normal responsivity either when measured with fMRI or with multi-unit recording. It is unlikely that the difference in these studies would be due to the use of fMRI as suggested by Calford et al. (Calford et al. 2005) because Chino et al. (Chen et al. 2012) found fMRI to be sensitive to subthreshold activity.

These studies recorded activity within three months of the lesion and we suggest that studies are needed to track the responsiveness of neurons over a longer time period. Early changes may be due to unmasking of latent inputs due to a loss of GABA (Garraghty and Kaas 1991) but there are also later changes in AMPA receptors (Garraghty et al. 2006) and in the morphology of the dendrites of neurons in the affected area (Churchill et al. 2004).

The second situation involves a lesion in part of the cortical map itself. Here there is no possibility that responsiveness could be regained within the lesioned area itself. However, after a partial lesion of V1 it is possible to record an increase in activity over time in the area adjacent to the lesion (Eysel 2009). After some time there is an increase in the size of the receptive fields of the neurons in the adjacent tissue. Possible mechanisms include a change in NMDA-receptor function (Yan et al. 2012).

The third situation involves changes of activity in higher sensory areas when they are deprived of part of their input by a lesion in earlier sensory areas. The result can depend on the stimulus used. For example, after a lesion in V1, neurons in MT still respond to the direction of moving bars (Rodman et al. 1989), but they no longer respond to the direction in random dot kinetogram (RDK) displays (Azzopardi and Cowey 2001). However, there is evidence that neurons adjacent to the region of MT that has lost its retinotopic input may show changes in their receptive fields and the deprived part of MT may regain a limited ability to respond to stimulation of the intact part of V1 (Collins et al. 2003).

These findings raise four questions relating to the recovery of performance on a motion task that can occur in patients with cortical lesions {Vaina, 2001 #7495}. The first is whether changes of the sort reported in animals can be found in patients with lesions in early sensory areas. We had the opportunity to study a patient (JS) with a localized unilateral infarct that involved the upper quadrant of V1 to V2v and VP. The patient was tested on his ability to discriminate the direction of motion in RDK displays where a variable proportion of dots provided motion signal (direction) while the others, masking motion noise. When the displays were presented to the affected quadrant he was extremely impaired at first, but with repeated testing over an eleven month period, his threshold improved to a normal or better than normal level. In the quadrant corresponding to the normal hemisphere, he was also somewhat impaired at first, but his performance became normal at three months after the lesion (Figure 2A)

We scanned this patient with fMRI at three, eight and eleven months post-infarct and mapped the early visual areas in the occipital lobes to see if there were changes in his retinotopy over this period and the area hMT+ that was not involved in his lesion, but is involved in processing the visual motion stimulus he was trained on. We also looked at his visual retinotopic map, not only for changes in size of retinotopic areas but also for displacement, since shifts have been reported after cortical dysgenesis {Slotnick, 2002 #28985}. We scanned repeatedly due to suggestions in the animal literature that changes in mapping after deafferentation can occur progressively and over a similar time period (Churchill et al. 1998). We were thus able to see whether changes also occur after a cortical lesion in humans. We also scanned three healthy controls who were trained on the same

motion task as patient JS to check whether similar changes could be detected in the absence of a lesion.

The second question is what effect any changes in retinotopic organization have on processing in higher visual areas that are involved in detecting direction in motion coherence stimuli, even if these areas are not involved in the lesion. We used fMRI to see if we could detect any changes in the responsive area of hMT+ that occurred with repeated testing. By scanning while the subjects responded to RDK displays we could see if there were any changes over time in the BOLD response.

The third question is whether the changes observed can account for the recovery that is seen in the performance of patient JS on the visual motion tasks. As described above, we gathered information on behavioural recovery, changes in retinotopic areas and changes in the BOLD signal in area MT+. Our interest was to determine whether, by combining this information, we would be able to establish a link between the physiological changes observed and the behavioral recovery exhibited by the patient.

The final question is whether the changes occur spontaneously or whether they can be promoted by formal training. Eysel (Eysel 2009) reported that repeated visual stimulation could induce more rapid change in the receptive fields after a visual cortical lesion. We addressed this question retrospectively in a patient (PF) that we had studied and who had a comparable lesion. Patient PF had a left occipital lobe infarct in V1 that extended significantly into V2v, the upper right quadrant of his visual field. This patient had not been involved in retraining on the motion coherence task, or any other task. He had been scanned at three and seven months. We were thus able to see whether there were changes in the retinotopic areas that were comparable with those seen in the first two scans obtained on patient JS.

Methods

Subjects

We studied seven right handed male subjects between 23 and 42 years old. Two were patients who had had single strokes, and the other five were healthy controls. All were alert, cooperative, and good at maintaining fixation on the psychophysical studies. All had normal or corrected-to-normal visual acuity.

Patient JS (25 y.o.) had a unilateral occipital infarct in the right hemisphere and patient PF (42 y.o.) had had a unilateral occipital infarct in the left hemisphere (Figure 1A,B).

Both patients had an upper quadrantanopia in the visual field contralateral to the lesion. The lesion in patient JS affected the right occipital cortex in the lingual gyrus and cuneus (Figure 1A), the lesion in patient PF produced cortical damage in the left lingual gyrus (Figure 1B). The infarct was caused in these patients by inadequate closure of the atrial septum in the heart (Patent Foramen Ovale); this was their only medically relevant problem.

After the infarct the patients underwent complete neuro-ophthalmological evaluations, including visual field tests using automated Humphrey perimetry, repeated twice and performed by the same technician (see Figure 1C&D). The patients complained of difficulties with several aspects of visual perception including visual motion. On formal testing with a subset of our motion stimuli, JS and PF were initially impaired on discrimination of direction and motion discontinuity tested with random dot kinematograms displays where a variable proportion of the dots provided directional information, that is signal, while the rest were nondirectional and so constituted noise (Newsome and Paré 1988; Vaina et al. 1990; Vaina et al. 2001).

All procedures were carried out in accordance with the Declaration of Helsinki and were approved by the Institutional Review Boards of Boston University and Athinoula Martinos Center for Biomedical Imaging, Massachusetts General Hospital, Harvard University. Participants were informed of the psychophysical and fMRI procedures and written informed consent was obtained.

Stimulus and Experimental Methods

Psychophysics—Random dot kinematogram (RDK) stimuli were generated using the C programming language in conjunction with the Video toolbox (Pelli 1997) and MacGLib 2.0 (Micro ML Inc., Québec, Canada) programming libraries, and were displayed with an Apple computer and 18" Apple CRT. The stimuli were adapted from Newsome and Pare (Newsome and Paré 1988) and Vaina et al. (Vaina et al. 1990; Vaina et al. 2001). They were random dot kinematograms (RDKs) composed of randomly positioned dots (6 arcmin in diameter; with a density of 2 dots/deg²) displayed in an imaginary circle of gray background and having a correlated motion signal of variable strength embedded in masking motion noise (Fig 2B). The dots were high-contrast black on a medium gray background to avoid the confound of light scatter. Dots that travelled outside the circular aperture were replotted at the opposite edge of the aperture to keep dot density constant.

Contrast, mean luminance, and spatial and temporal frequency content did not change in the RDK stimuli. The speed of motion was 3°/sec, defined as the distance a signal dot was displaced between successive frames. These types of displays have been used for more than twenty years in our laboratory in several psychophysical motion tasks both with healthy subjects and stroke patients. They have also been used in experiments in which hMT+ has been localized with fMRI.

Motion Coherence—RDKs were presented within a 6° imaginary aperture with the properties described above. A variable proportion of the dots constituted the signal, moving coherently in one of the cardinal directions (up, down, left or right); the remainder dots were repositioned between frames to provide masking motion noise. Signal dots were chosen independently on each frame, so that individual dots could not be tracked to determine direction, since it was unknown which dots would be signal on any given frame. We used an adaptive staircase procedure (Vaina et al. 2003) to determine the percentage of signal dots to determine response threshold. The subjects' task was to determine in a four-alternatives forced choice (4AFC) whether the global direction of the RDK appeared to be up, down,

left, or right. A schematic of the stimulus is shown in Figure 2B. The subjects were asked to respond as soon as possible and as accurately as possible.

Motion Discontinuity—The RDK was displayed in a 6° circular aperture with the properties described above. In a 2AFC task subjects were asked to determine whether the display was homogeneous as in the motion coherence test or if it had an illusory edge or discontinuity passing through the center of the display. This discontinuity was defined by the difference in direction of the signal dots, with half of the display signal dots moving upwards, and the other half moving downwards. The illusory edge was randomly chosen to be horizontal, vertical or diagonal. A schematic of the test is shown in Figure 3B. Again the subjects were asked to respond as soon as possible and as accurately as possible.

Behavioral training—Patient JS was trained on the Motion Coherence test for eight months, twice weekly, for 300 trials each time. All motion stimuli were presented 2° off the border of the horizontal and vertical meridians so as to fall on a preselected location in the upper left (affected) or upper right (unaffected) visual field quadrant. Fixation was at the center of the screen. In each training session, two thresholds were obtained on the motion coherence test and these were averaged to determine the coherence level for training. During training, trials were presented at each of three coherence levels in a randomized sequence: threshold, and plus and minus standard deviation. Towards the end of training, when the performance of JS improved significantly, the threshold coherence or standard deviations were too small and so we used threshold and plus/minus 4–5% coherence levels. No feedback was ever given as to the correctness of the response. Neither patient PF nor the healthy control subjects underwent training on this task.

Patient JS was also given on several occasions the Motion Discontinuity task. He performed the task one week prior to the first fMRI scan, as well on two training days, during the same visits as two MCT training sessions, prior to the second fMRI scan, and again a final time after the second scan.

MR Scanning

Schedule of scans—The fMRI scans were repeated approximately 6 months apart in three of the healthy controls and in the two patients. Patient JS was scanned three times, at 3, 8, and 11 months after the infarct, and Patient PF twice, at 3 and 7 months after the infarct. Controls and both patients underwent retinotopic mapping in each scan.

Patient JS was performed the Motion Coherence task at all three of his scans, and the Motion Discontinuity task at two of the scans. We focused on area human MT+ (hMT+) since this has been shown to be activated on tasks that involve motion coherence stimuli (Vaina et al. 1990; Vaina et al. 2001). In the Motion Discontinuity task we also focused on the lateral occipital area KO or V3B. This is involved in extracting edges that are defined by difference in motion (Dupont et al. 1997; Van Oostende et al. 1997) and also in the analysis of optic flow (Greenlee 2000; Rutschmann et al. 2000).

During fMRI the motion-coherence stimulus subtended 12° diameter and was presented in the central visual field and central fixation. As in the psychophysical testing and training,

this was a 4AFC task: in the stimulus periods, the strength of the motion signal was determined by the proportion of correlated dots or signal dots that were displaced between frames by a fixed spatial offset in one of four cardinal directions, up, down, left up. The remaining dots (noise dots) were positioned randomly within the aperture.

The Motion Discontinuity test used in fMRI was identical to the one administered during psychophysical testing. During scanning, the stimulus was placed in the upper ipsilesional or upper contralesional quadrant, with its edge positioned 2° off the vertical and horizontal meridians. The stimulus location, that is the quadrant of presentation, was counter-balanced across 6 runs.

In both tasks during stimulus presentation (the ON period), a new stimulus was displayed every second. In the OFF period, the display contained only noise dots forming a fluctuating pattern of spatiotemporal white noise. The levels of coherence (proportion signal dots) in the ON period were determined prior to scanning based on the subjects' threshold obtained by administering the test through the staircase method.

Image acquisition—All imaging was done at the Martinos Center for Biomedical Imaging, Massachusetts general Hospital on a 3.0T Siemens Trio high-speed echo-planar imaging device (Siemens Ltd., Erlangen, Germany) with a quadrature head coil. During scanning subjects were fitted with earplugs. They lay supine within the bore of the magnet with a forehead strap and foam pads placed tightly around the ears and head to minimize head motion. Head motion was detected and corrected using the Martinos Center's automatic image registration (AIR) algorithm (Woods et al. 1992).

In both patients and healthy control we obtained two conventional high resolution 3D T1 weighted MPRAGE anatomical images, for 6.5 min each. There were 1mm isotropic voxels, with a repetition time [TR] of 2530ms, an echo time [TE] of 3.49ms and a flip angle of 7 degrees. The anatomical scans were used for cortical surface reconstruction, and for registering the functional scans to the subject's anatomy. In the two patients we also acquired a high resolution isotropic (1mm) set of T2-Space MRI images for lesion localization with a TR of 3200ms and a TE of 839ms. All structural images are obtained in NIFTI format which were used with MRICron (<http://www.sph.sc.edu/comd/rorden/mricron/>) for lesion visualization. The fMRI data were analyzed and visualized using MEDx, FS-Fast and Freesurfer.

Special gradient echo EPI sequences (Siemen's PACE sequences), which follow closely the motion of the head, were used to reduce head motion artifacts and scanner drift. The Siemens autoalign protocol developed by van der Kouve at the Martino's Center was used in each fMRI scanning to assure the registration of the imaged slices to the location of a predetermined brain template (<http://www.nmr.mgh.harvard.edu/~andre/Autoalign/Autoalign-instructions.html>). This guarantees that a subject will be scanned at the same slice positions in every run and every new scanning session. A field shimming procedure was used to minimize magnetic susceptibility distortions (Reese et al. 1995).

Whole brain functional MR images were acquired using gradient echo planar imaging (EPI) sequences for measurement of BOLD signals. In patient JS and controls, the functional BOLD image volume constituted 22 contiguous 5mm-thick slices with a 1mm gap and a field of view of 20×20 cm. The TR was 2.5 s and the TE 70 ms, with a flip angle of 90 degrees. In patient PF the functional BOLD image volume consisted of 33 contiguous 3.6 mm-thick slices with no gap and field of view of 20×20 cm. The TR was 2 s and the TE = 30 ms, with a flip angle of 90 degrees.

Analysis of fMRI data on the behavioral tasks—No spatial or temporal smoothing was performed on the data. The functional data on the behavioral tasks in patient JS was analysed using the MEDx 3.4.2 software package (Sensor Systems, Sterling Va) and additional scripts developed in our lab in MATLAB and Perl. We used a blocked design paradigm consisting of eight 20s OFF periods and seven 20s ON periods, interleaved. The ON period consisted of a series of Motion Coherence or Motion Discontinuity displays as described above, while the OFF period contained noise dots matched to all the stimulus properties (density, size, luminance, speed).

Initial steps of the analysis followed our previously published methods (Vaina et al. 2001; Vaina and Soloviev 2004). Briefly, active brain regions were determined by means of a t-test comparison of the ON and OFF periods of the experimental paradigm. Timing of each paradigm condition was automatically recorded during each fMRI scan, and the first four frames were removed from each acquisition to compensate for the effects of adaptation of a subject to the start of a new experimental run. A 5s delay was introduced into each paradigm file to account for the effects of hydrodynamic delay in fMRI responses. A statistical significance threshold of $p < 0.05$ (resel corrected) was applied to the data with an extent threshold of a minimum cluster size of five voxels (Worsley et al. 1992; Worsley et al. 1996). For each subject, EPI images were registered to the high-resolution de-skulled structural volume. The same transformation was applied to the statistical data. Thresholded statistical maps were superimposed onto a high resolution structural volume.

Area MT+ was localized in JS by aligning the activation on the Motion Coherence task with the high-resolution structural brain volume.

Lesion localization—In both patients, we used the MRICron software package (<http://www.sph.sc.edu/comd/rorden/mricron>) to localize and visualize the lesions. Lesions were drawn manually on axial slices, and the brains were transformed to MNI space (Montreal Neurological Institute). Axial slice views of the lesions are shown in Figure 1A&B, with slices chosen to span the extent of the lesions (z -coordinates of -9 to $+18$ in JS and -16 to $+8$ in PF). Their location in the occipital lobes is illustrated on a sagittal slice for each patient, in the last panel in Figure 1A&B.

The lesion in patient JS was in the right hemisphere. It was subtotal in V1 and it extended into the ventral visual stream, including V2v and VP. The lesion in patient PF was in the left hemisphere. It was also subtotal in V1 but it included almost all of V2v in the ventral visual stream.

Retinotopic mapping—As already mentioned, retinotopic mapping was carried out three times in Patient JS and twice in patient PF. The data for patient JS were analyzed using the 3D phase-encoded retinotopic mapping technique of Dumoulin et al. (Dumoulin et al. 2003). This has the advantage that it does not require the reconstruction of the cortical surface. In this method the visual field sign identification is completely automatic and the method directly supplies volumes for a region-of-interest analysis.

The power spectrum of each voxel's time-series was computed by a discrete Fourier transform and used in the construction of two phase-maps. One was created by taking the phase of the fundamental frequency varied as a function of polar-angle when the stimulus was the rotating wedge and the other by taking the phase of the fundamental frequency varied as a function of eccentricity when stimulus was expanding rings. The t-statistical maps were created using a Spearman rank order test for each voxel, with the phase taken from the corresponding phase map.

To calculate the field sign map, three partial derivative maps were used, for polar-angle, eccentricity and cortex. These were computed by convolving the volumes with the partial derivative of a Gaussian kernel. The partial derivative map identifies the cortical surface normals. The visual sign map (VFS) was multiplied by the t-statistical map to create a weighted map of the visual field sign computation (tVFS). The absolute values in the resulting maps indicate a statistical certainty of the visual field sign computation (Dumoulin et al. 2003). Retinotopic areas were identified in the tVFS map by manually outlining and labeling retinotopic areas on the reconstructed brain surface and the tVFS map, starting with area V1, centered around the calcarine sulcus and having negative field sign, and extending both ventrally and dorsally into the higher areas.

To estimate the volume of a retinotopic ROI, we multiplied the number of voxels inside the ROI by the volume of the voxel. We further computed the surface based coordinates using routines from Free Surfer (<https://surfer.nmr.mgh.harvard.edu>). Specifically, the retinotopic ROIs were manually labeled on a 2-D flat map using FreeSurfer, where each ROI consisted of a set of the nearest nodes on a mesh describing the boundary of the white-gray matter interface. Mesh nodes are the vertices of the triangular patches that form 3-D cortical manifold obtained in brain surface reconstruction. The area of a ROI is simply the sum of the area of each of triangles (Dale et al. 1999; Fischl et al. 1999; Fischl et al. 2001).

Retinotopic mapping was also obtained on patient PF. As explained in the introduction he was chosen retrospectively to see whether changes in retinotopic organization could also be observed after the lesion in absence of formal training on visual tasks. In Patient PF, retinotopic analysis had been performed using the standard techniques incorporated in Freesurfer (Engel et al. 1994; Sereno et al. 1995; DeYoe et al. 1996; Engel et al. 1997).

Measuring changes in retinotopic visual areas—To assess quantitatively changes in Patient JS's retinotopic maps over three fMRI scans obtained at 3, 8 and 11 months after the infarct, during which he underwent training on the motion coherence task, we projected the ROI boundaries and center positions into spherical coordinates. From this, we estimated the geodesic distances on the gray/white matter boundary surface in surface-based coordinate

system (Fischl et al. 1999) by computing the arc along the great circle connecting two points (the centers of mass of each ROI assessed in consecutive scans):

$$ds^2 = (d\theta^2 + \sin^2(\theta)d\phi^2)r^2$$

where θ is the azimuthal angle in the xy -plane from the x -axis with $0 \leq \theta < 2\pi$, a longitude, and ϕ is the polar angle from the z -axis with $0 \leq \phi \leq \pi$, a colatitude. The resulting measurement provides the distance along the cortical surface (in mm) between two points, allowing us to assess the distance which an ROI's center of mass shifted between scans. The typical error of estimating distance on the cortex is estimated to be around 10–15% (Fischl et al. 1999).

Voxel-based correlation of functional responses across scans—To further assess the changes in patterns of organization and response between scans, we computed a voxel-wise correlation analysis within each retinotopic area based on the BOLD response to a full-field checkerboard stimulus. We measured the BOLD % signal change for each voxel in a given ROI in each of two successive fMRI scans. All voxels in an ROI of the earlier scan were included, even if they were classified within a different retinotopic area in the next scan. We measured the correlation in BOLD response among voxels having positive BOLD signal percent change to determine how stimulus-responsive cortical voxels changed in their responses between scans. Correlation was assessed using a Pearson linear correlation factor, with each data point representing a single voxel.

Results

Behavioral performance

Motion coherence task—Figure 2 shows the thresholds for JS during the course of training on this task, obtained from an adaptive staircase (Vaina et al. 2003) at the start of each training sessions. At first JS failed for the stimuli presented to the upper left (affected) quadrant. However, he could achieve a coherence level of roughly 30% if the stimuli were presented to his upper right (unaffected) quadrant, but this level of performance was significantly worse than for the control subjects whose thresholds were around 7% ($z = 9.05$, $p < 0.001$). In the first 5–12 weeks JS's performance improved significantly across sessions in both the contralesional ($F = 31.54$, $p = 0.0025$) and ipsilesional quadrant ($F = 27.08$, $p = 0.002$), reaching 30% and 20% respectively. At this stage his threshold for central vision was also around 20%, and this was used to guide the choice of constant stimuli during the first fMRI session (15%, 20%, 25% coherence).

Training continued in the interval between the first and second fMRI scans. Figure 2A shows examples of thresholds obtained on the training days, illustrated in weekly intervals. For stimuli shown in the left upper quadrant contralateral to the lesion there was an initial drop in the threshold indicating some improvement in performance. However performance between 3–8 months after the lesion remained relatively flat ($F = 5.8$, $p > 0.05$). Again the threshold for coherence for stimuli presented in the central visual field obtained at 8 months

after the lesion guided the choice of coherence values in the centrally presented stimulus in the second fMRI.

In the third segment of training (8–11mo) there were 17 training sessions, and thresholds for stimuli shown in both upper visual field quadrants were very similar. They show that performance improved significantly in both the left ($F = 30.53$, $p < 0.001$) and right ($F = 10.95$, $p = 0.01$) visual fields to below 5% coherence in both quadrants. This level of performance was actually slightly better than that of the healthy controls. Before the third fMRI the central fixation threshold was obtained to guide the choice of the constant stimuli in the scanner (4%, 8%, 12%).

Motion discontinuity task—Figure 3 shows the performance of JS on the motion discontinuity task. JS was tested on this task once one week prior to the first fMRI scan, then twice on the same days as two training sessions on motion coherence prior to the second fMRI scan, and again after the second scan. He was initially severely impaired on the task compared with the controls. However, when tested before the second fMRI scan, his thresholds were much lower and similar to the threshold at that time on the motion coherence task. This suggests that the improvement on the motion discontinuity task was due to training on motion coherence such that he was better tuned to the signal provided by the coherent dots.

fMRI during performance of motion tasks

Motion coherence task—Figure 2C shows the activations for V1 and hMT+ for JS. The display was presented to the central visual field. Data are also presented for a control subject who was tested two times. In JS the number of active voxels in V1 increased over the three tests. The volume of the activated V1 was 0.05cm^3 at three months after the lesion and 0.31cm^3 at eleven months after the lesion. There was no significant change in the volume of the activated V1 in the control subject.

In JS, the total volume of active voxels in hMT+ decreased over time in the normal left hemisphere (from 0.86cm^3 at 3mo, to 0.64cm^3 at 11mo). Furthermore, the mean BOLD signal percent change for active voxels ($Z > 3.0$) decreased from 1.51% in the first scan to 0.99% in the third scan. There was no such change in the right (lesioned) hemisphere or in the control subject. The value of 0.99% for JS in the third scan is similar to the values of 0.91% in the right and 0.87% in the left hemisphere for the control subject.

Motion discontinuity task—Patient JS performed the MDT task at both the 3 and 8 mo scans, during which time his performance on both MCT and MDT improved dramatically, as shown above. MDT was administered in both the upper right (unaffected) and left (affected) visual field quadrants, in the same locations as they were presented psychophysically. Figure 4 shows the activations for the area MT+ and also for the earlier visual area KO/V3B in response to the MDT task.

In a control subject (Figure 4, bottom row), we found that the task primarily activated the contralateral hMT+ and KO, while also minorly activating the ipsilateral hMT+. Contralateral hMT+ activity engaged a surface area of 6.50cm^3 in the URVF (LH hMT+)

and 5.57 cm³ in the ULVF (RH hMT+), compared to 3.22 and 5.51 cm³ area of activation for the ipsilateral hMT+ in the URVF and ULVF respectively. Activation in KO was seen contralaterally (4.86 and 3.63 cm³ for URVF and ULVF respectively), but there was no ipsilateral activation in response to either visual field condition.

Figure 4B shows the data for the upper right (unaffected) quadrant for patient JS. Similar to controls, in both scans JS showed activation in MT+ in both hemispheres (14.65 and 10.84 cm³ in LH hMT+, 4.75 and 5.04 in RH hMT+ for the 3 and 8mo scans, respectively) as well as in contralateral (LH) KO (4.10, 4.63 cm³), but did not activate ipsilateral KO.

Figure 4A shows the data for the upper left (affected) quadrant. In the first scan, there was activation ($Z > 3$) in hMT+ in both the right (lesioned, 6.80 cm³) and left hemisphere (5.86 cm³) of JS, but no activation was seen in either KO. In the second scan, the activation extent in hMT+ had increased in both the right and left hemisphere in JS (to 10.49 and 6.15 cm³, respectively). Interestingly, although no activation was seen in either hemisphere's KO during the first scan, in the second scan both hemispheres showed significant KO activation (4.92 and 5.92 cm³, in the LH and RH respectively). This recruitment of bilateral KO activation occurred simultaneously to the subject's improvement on the (untrained) MDT task and the (trained) MCT task.

Retinotopic mapping

Patient JS—Figure 5 shows the retinotopic areas for patient JS in the scans at three, eight and eleven months after his infarct. For each scan, we measured the size and center of mass of each retinotopic area. To arrive at a quantitative assessment of the change in the surface of the areas, we used the intact hemisphere as a reference and measured the extent in the ipsilesional and contralesional hemisphere. Table 1 presents the data for the ipsilesional / contralesional (I/C) ratio for each area. We used the center of mass of each area to determine whether there was a shift across scans (over time).

In the initial scan, there was a significant reduction in the activated area of V1, V2v and VP in the lesioned compared to JS's normal hemisphere, with I/C ratios of 0.37, 0.19 and 0.21 respectively. There was also a minor reduction in V2d with an I/C ratio of 0.58. The reduction was expected for areas V1, V2v and VP because they were involved in the lesion. The reduction in the V2d could either be due to damage that is not evident or to a loss of input from earlier areas.

Over the course of the following months, there was substantial recovery of surface area in all these areas (Table 1). The I/C ratio for V1 increased from 0.37 to 0.48 to 0.52 over the 3 scans. The corresponding ratios for area V2v were 0.19, 0.17 and 0.52, and for area V2d 0.58, 0.59 and 0.74. Area VP or V3v also increased progressively over the three scans, from 0.21 to 0.40 to 0.48.

The pattern was different for the retinotopic areas that are higher in the hierarchy of visual processing. Initially, areas V4 in the ventral stream and V3 in the dorsal stream were as extensive in the right as the left hemisphere, and V3a in the dorsal stream was more extensive in the right hemisphere. In the first scan, the I/C ratios in these areas were 0.85,

0.94 and 1.57 respectively. However, by the third scan the I/C ratios were reduced to 0.66, 0.38 and 0.79 respectively.

Given all these changes, we were interested in whether there were also shifts in the center of mass of each ROI. We measured the shift along the cortical surface using a spherical coordinate projection. This is as shown in Figure 6A and as described in the Methods.

Figure 6 illustrates the magnitude of shifts of the center of mass in each retinotopic areas in the lesioned (right) hemisphere. In several ROIs the shift of the center of mass was consistent with the changes in surface area as reported in Table 1. These shifts were most marked between eight and eleven months. In the time between the first and second scans only area VP showed a significantly larger shift, of 3.8mm, than in the intact hemisphere and in the normal controls. (Table 2). However, in the interval between the second and third scans, there were shifts ranging from 1.7mm in V2v to 6.9mm in V3 (Figure 6, Table 2). By contrast in the intact left hemisphere of patient JS the shifts were small with a maximum of 1.5mm and they did not show any systematic pattern. Furthermore, in the control subject the shifts were negligible, of the order of less than 0.5mm (Table 2).

This trend is also seen in the retinotopic occipital areas in the analysis of the correlations between the BOLD responses of voxels across scans in the full field checkerboard stimulus (Table 3). We used voxel-wise correlation in the BOLD response to a full-field checkerboard stimulus to examine the consistency of responses of voxels in retinotopic areas V2v, V2d and V3/VP (Figure 7 and Table 3). In the lesioned right hemisphere the variability in response between the 3 and 8 month scans was much higher compared to the control subject in both V2d ($r_R=0.4$) and V2v ($r_R=0.2$), but it was largely reduced between the 8 and 11 month scans ($r_R=0.7$, 0.4 for V2d and V2v), and almost no variability was observed in the intact, left hemisphere ($r_L \geq 0.8$ for V2d and V2v in both intervals). These results suggest that the weak correlations were specific to the damaged hemisphere and were observed mainly within the scans performed within the first 8 months following stroke.

In areas V3 and VP, we again found weakened correlations in JS' lesioned right hemisphere (but not in the normal left hemisphere) compared to the control (Table 3), but unlike V2d/v, the correlations did not improve between the later scans. The consistency in activation in area V3 decreased ($r_R=0.8$ to 0.5) over the later time period (8 to 11 months). Thus, whereas V2d/v showed a return to higher activation consistency after 8 months, V3 and VP continued to show a high degree of variability.

Patient PF—In this patient the lesion was in the left hemisphere. In this patient, therefore the I/C ratio compares the areas in the left (ipsilesional) with the right (contralesional) hemisphere. As in patient JS, the lesion extended from V1 to V2v, but as can be seen from Figure 4, area V2v was almost completely eradicated in the left hemisphere

Figure 8 shows the results for retinotopic mapping and Table 1 gives the I/C ratios for the two scans. Initially, the area of activated V1 was slightly reduced in size with an I/C of 0.88, but there was almost no evidence of an activated V2v in the affected hemisphere with an I/C ratio of 0.08). However, by the second scan, the ratio for V1 was 1.71; in other words

the activated V1 was now larger in the affected hemisphere. The results for V2v remained unchanged.

By the second scan there was a significant increase in the I/C ratio of V2d; the ratio was 0.62 at scan 1 and 1.66 at scan 2. As in patient JS there were decreases in some areas later in the hierarchy of visual processing. The ratios for VP or V3v went from 1.31 to 0.84, and for V3 from 1.12 to 0.98.

Discussion

The introduction asked four questions. The first was whether the sort of changes reported in animals after lesions can be found in patients. It is clear that they can. Eysel et al. (Eysel 2009) found that after a striate lesion in cats there is an increase in the receptive fields of neurons adjacent to the lesion. Zepeda et al. (Zepeda et al. 2003; Zepeda et al. 2004) used both cell recording and optical imaging to show that after a striate lesion in kittens there is an expansion in the representation of visual space in the surrounding area.

We studied patient JS who has a lesion in V1, extending into V2v and VP. This lesion caused an upper left quadrantanopia (Figure 1C) consistent with his ventral, occipital lobe lesion. As in the experiments by Zepeda et al. on cats there was a decrease at first in the extent of V1 in the lesioned hemisphere, but with time this area increased markedly. The increase continued over a period of eleven months after the infarct.

The spatial resolution of fMRI is not good enough to make a definitive judgement about where within V1 the changes occurred. However, fMRI has the advantage over single unit recording that it is a whole brain method. This means that we have been able to show that similar changes occurred in the other areas on which the lesion encroached. In the case of JS, these were V2v and VP. There was also an increase in these areas over time.

These increases appear to have been at the expense of adjacent areas. We noted significant decreases in V3 and V3a. Baseler et al. (Baseler et al. 1999) have suggested that, when neurons in an area lose their normal inputs, they can be 'colonized' by other neurons in neighbouring cortex, meaning that they can become responsive to new inputs. Baseler et al. further suggest that this effect is mediated by horizontal connections. They carried out retinotopic mapping in a patient with a large lesion of V1 that extended into V2v and VP and report reorganization of the retinotopy in V2d and V3d. While colonization of this sort might occur between neurons within an area, further research is needed to see if it can occur for neurons in different areas.

To document the retinotopic changes we have compared the size of the different areas in the lesioned and non lesioned hemisphere (Table 1). This has the advantage that the non-lesioned hemisphere acts as a control, thus providing a measure of the test-retest reliability of the mapping. Though such a test is also provided by retinotopic mapping in healthy subjects, the use of the non lesioned hemisphere in patients serves as a more rigorous test since it is carried out in an abnormal brain.

These changes could, however, be explained in a different way. Though we did not add smoothing there is spatial smoothing in the pre-processing of the fMRI data, and a change in the amplitude of the signal can appear as a change in extent. Yet we noted shifts of the order of five millimeters or more, and it is not clear how the shift in the center of mass can be explained in this way. We conclude that there were genuine changes in retinotopy that were not simply the result of changes in responsivity.

In addition to the shifts in retinotopic area location, we assessed correlation in the functional responses to a full-field checkerboard stimulus by voxels within various retinotopic ROIs across scans. This data showed significant reductions in response correlation in the damaged hemisphere's V2d/v between the 3 and 8 month scans, and in V3 and VP in the damaged hemisphere, persisting beyond 8 months post-infarct. The time frame for reorganization in the areas V2d/v was restricted to the time interval between the first two scans (3 and 8 months), as shown by the since substantially reduced correlations between these time points. Negligible changes were seen between 8 and 11 months. On the other hand, correlations in V3 and VP remained low throughout, suggesting continued reorganization after the 8 month mark. Further data is needed to more fully assess these points, but they are suggestive of lesion-driven plasticity in visual cortex in conjunction with the changes in ROI area and location, and point to specific time frames over which such changes occur.

The second question posed in the introduction was what effect any changes in early visual areas have on the activity of higher areas involved in detecting the direction in motion coherence displays. Collins et al. (Collins et al. 2003) recorded in MT in monkeys with subtotal striate lesions, and found that neurons in the deprived zone did not respond to coherent motion. However, they suggest that some partially deprived neurons may have acquired new receptive fields. Rosa et al. (Rosa et al. 2000) also reported that there were neurons in the deprived zone that had displaced receptive fields. Functional imaging does not have the spatial resolution to detect the border of the deprived zone. However, as already mentioned it has the advantage of being a whole brain method. In patient JS there was an increase in the BOLD signal in both MT+ and KO in the lesioned hemisphere when performance improved on the Motion Discontinuity task (Figure 3). Here the BOLD response was the result of a comparison between the motion signal and noise.

The third question is whether the changes observed can account for the recovery. There were two changes in earlier retinotopic areas in patient JS. The first was the increase in the area of responsivity in the lesioned region, including V1, when tested with the rotating wedge and expanding rings. The second was the very significant increase in the area of responsiveness in V1 over the three scans when the patient was presented with the motion coherence displays. To find out whether the retinotopic changes are necessary for the recovery, one would need to see if there are cases of recovery but no changes in retinotopy, or if there are cases of changes in retinotopy but no recovery. Further research is therefore needed to discover if it possible to establish cause and effect.

The final question was whether training promotes recovery. As explained in the introduction we tried to tackle this question by finding a patient with a similar lesion who had not been formally trained on the motion tasks. Unfortunately, because patient PF was chosen

retrospectively, the methods for analyzing the retinotopic mapping were not identical to those used with patient JS. As explained in the methods section the technique devised by Dumoulin (Dumoulin et al. 2003) was used with JS but not with PF. Nonetheless we take it as significant that in patient PF there were marked changes in retinotopy over time. However, this patient was only tested at three and six months after the infarct, while the largest shifts in patient JS occurred between eight to eleven months after the infarct. It could be that these simply correspond to the third stage of recovery described by Churchill et al. (Churchill et al. 1998), but we cannot discount the possibility that they were promoted by formal training on the motion coherence task.

That training might have such an effect is suggested by the nature of the mechanisms that underlie the changes in responsiveness over time. After a stroke there are physiological changes such that neurons become more excitable and susceptible to LTP (Carmichael 2003). Furthermore, there is speculation that there are common mechanisms for the cortical changes that occur with injury, activity and experience (Overman and Carmichael 2013). There are even suggestions that changes in cortex may recapitulate ones that occur early in development (Mowery and Garraghty 2009). If so, training might indeed promote the rebuilding of circuits.

That it might do so is not the same as saying that we know that it does so. Nor do we pretend to have carried out a proper test of the effects of training. In everyday life patient PF would have been exposed to visual experiences that might promote cortical changes. However, we distinguish such experience from the potential effects of formal training such as that received by patient JS. It would clearly be worth carrying out a proper trial in which retinotopic mapping is performed repeatedly as in the present paper, but with two groups of patients of which one is trained and the other is not.

Acknowledgements

This work was supported by NIH grant R01NS064100 to L.M.V.

References

- Azzopardi P, Cowey A. Motion discrimination in cortically blind patients. *Brain; a Journal of Neurology*. 2001; 124:30–46.
- Baseler HA, Morland AB, Wandell BA. Topographic organization of human visual areas in the absence of input from primary cortex. *J Neurosci*. 1999; 19:2619–2627. [PubMed: 10087075]
- Calford MB, Chino YM, Das A, et al. Neuroscience: rewiring the adult brain. *Nature*. 2005; 438:E3. discussion E3–4. [PubMed: 16280984]
- Carmichael ST. Plasticity of cortical projections after stroke. *Neuroscientist*. 2003; 9:64–75. [PubMed: 12580341]
- Chen LM, Qi HX, Kaas JH. Dynamic reorganization of digit representations in somatosensory cortex of nonhuman primates after spinal cord injury. *J Neurosci*. 2012; 32:14649–14663. [PubMed: 23077051]
- Chino YM. Adult plasticity in the visual system. *Can J Physiol Pharmacol*. 1995; 73:1323–1338. [PubMed: 8748982]
- Churchill JD, Muja N, Myers WA, Besheer J, Garraghty PE. Somatotopic consolidation: a third phase of reorganization after peripheral nerve injury in adult squirrel monkeys. *Exp Brain Res*. 1998; 118:189–196. [PubMed: 9547087]

- Churchill JD, Tharp JA, Wellman CL, Sengelaub DR, Garraghty PE. Morphological correlates of injury-induced reorganization in primate somatosensory cortex. *BMC Neurosci.* 2004; 5:43. [PubMed: 15533258]
- Collins CE, Lyon DC, Kaas JH. Responses of neurons in the middle temporal visual area after long-standing lesions of the primary visual cortex in adult new world monkeys. *J Neurosci.* 2003; 23:2251–2264. [PubMed: 12657684]
- Dale AM, Fischl B, Sereno MI. Cortical surface-based analysis. I. Segmentation and surface reconstruction. *Neuroimage.* 1999; 9:179–194. [PubMed: 9931268]
- DeYoe EA, Carman GJ, Bandettini P, et al. Mapping striate and extrastriate visual areas in human cerebral cortex. *Proceedings of the National Academy of Science of U.S.A.* 93:2382–2386.
- Dumoulin SO, Hoge RD, Baker CL, Hess RF, Achtman RL, Evans AC. Automatic volumetric segmentation of human visual retinotopic cortex. *Neuroimage.* 2003; 18:576–587. [PubMed: 12667835]
- Dupont P, De Bruyn B, Vandenberghe R, et al. The kinetic occipital region in human visual cortex. *Cerebral Cortex.* 1997; 7:283–292. [PubMed: 9143447]
- Engel S, Rumelhart D, Wandell B, Lee A, Glover G, Chichilniski E, Shadlen M. fMRI of human visual cortex. *Nature.* 1994; 370:106. [PubMed: 8022478]
- Engel SA, Glover GH, Wandell BA. Retinotopic organization in human visual cortex and the spatial precision of functional MRI. *Cerebral Cortex.* 1997; 7:181–192. [PubMed: 9087826]
- Eysel, UT. *Adult Cortical Plasticity.* Elsevier Ltd.; 2009. p. 7
- Fischl B, Liu A, Dale AM. Automated manifold surgery: constructing geometrically accurate and topologically correct models of the human cerebral cortex. *IEEE Trans Med Imaging.* 2001; 20:70–80. [PubMed: 11293693]
- Fischl B, Sereno MI, Dale AM. Cortical surface-based analysis. II: Inflation, flattening, and a surface-based coordinate system. *Neuroimage.* 1999; 9:195–207. [PubMed: 9931269]
- Garraghty PE, Arnold LL, Wellman CL, Mowery TM. Receptor autoradiographic correlates of deafferentation-induced reorganization in adult primate somatosensory cortex. *J Comp Neurol.* 2006; 497:636–645. [PubMed: 16739196]
- Garraghty PE, Kaas JH. Large-scale functional reorganization in adult monkey cortex after peripheral nerve injury. *Proceedings of the National Academy of Sciences.* 1991; 88:6976–6980.
- Greenlee MW. Human Cortical areas underlying the perception of optic flow: brain imaging studies. *International Review of Neurobiology.* 2000; 44:269–292. [PubMed: 10605650]
- Huxlin KR, Martin T, Kelly K, Riley M, Friedman DI, Burgin WS, Hayhoe M. Perceptual relearning of complex visual motion after V1 damage in humans. *J Neurosci.* 2009; 29:3981–3991. [PubMed: 19339594]
- Jain N, Qi HX, Collins CE, Kaas JH. Large-scale reorganization in the somatosensory cortex and thalamus after sensory loss in macaque monkeys. *J Neurosci.* 2008; 28:11042–11060. [PubMed: 18945912]
- Merzenich MM, Nelson RJ, Stryker MP, Cynader MS, Schoppmann A, Zook JM. Somatosensory cortical map changes following digit amputation in adult monkeys. *J Comp Neurol.* 1984; 224:591–605. [PubMed: 6725633]
- Moore T, Rodman HR, Gross CG. Direction of motion discrimination after early lesions of striate cortex (V1) of the macaque monkey. *Proceeding of the National Academy of Sciences USA.* 2001; 98:325–330.
- Mowery TM, Garraghty PE. Nerve-Injury Induced Changes to GluR1 and GluR2/3 Sub-unit Expression in Area 3b of Adult Squirrel Monkeys: Developmental Recapitulation? *Front Syst Neurosci.* 2009; 3:1. [PubMed: 19212458]
- Newsome WT, Paré EB. A selective impairment of motion perception following lesions of the middle temporal visual area (MT). *Journal of Neuroscience.* 1988; 8:2201–2211. [PubMed: 3385495]
- Overman JJ, Carmichael ST. *Plasticity in the Injured Brain: More than Molecules Matter.* Neuroscientist. 2013
- Pelli DG. The VideoToolbox software for visual psychophysics: transforming numbers into movies. *Spat Vis.* 1997; 10:437–442. [PubMed: 9176953]

- Reese TG, Davis TL, Weisskoff RM. Automated shimming at 1.5 Tesla using echo planar image frequency maps. *Journal of magnetic resonance imaging*. 1995; 5:739–745. [PubMed: 8748496]
- Rodman HR, Gross CG, Albright TD. Afferent Basis of Visual Response Properties in Area MT of the Macaque. I. Effects of Striate Cortex Removal. *J Neurosci*. 1989; 9:2033–2050. [PubMed: 2723765]
- Rosa MG, Tweeddale R, Elston GN. Visual responses of neurons in the middle temporal area of new world monkeys after lesions of striate cortex. *J Neurosci*. 2000; 20:5552–5563. [PubMed: 10884339]
- Rutschmann R, Schrauf M, Greenlee MW. Brain activation during dichoptic presentation of optic flow stimuli. *Experimental Brain Research*. 2000; 134:533–537. [PubMed: 11081835]
- Sereno MI, Dale AM, Reppas JB, et al. Borders of multiple visual areas in humans revealed by functional magnetic resonance imaging. *Science*. 1995; 268:889–893. [PubMed: 7754376]
- Smirnakis SM, Brewer AA, Schmid MC, et al. Lack of long-term cortical reorganization after macaque retinal lesions. *Nature*. 2005; 435:300–307. [PubMed: 15902248]
- Vaina LM, Cowey A, Eskew RT, LeMay M, Kemper T. Regional cerebral correlates of global motion perception: Evidence from unilateral cerebral brain damage. *Brain*. 2001; 124:310–321. [PubMed: 11157558]
- Vaina LM, Gryzwacz NM, Saiviroonporn P, LeMay M, Bienfang DC, Cowey A. Can spatial and temporal motion integration compensate for deficits in local motion mechanisms? *Neuropsychologia*. 2003; 41:1817–1836. [PubMed: 14527545]
- Vaina LM, LeMay M, Bienfang DC, Choi AY, Nakayama K. Intact "biological motion" and "structure from motion" perception in a patient with impaired motion mechanisms: a case study. *Visual Neuroscience*. 1990; 5:353–369. [PubMed: 2265150]
- Vaina, LM.; Soloviev, S. Functional neuroanatomy of self-motion perception in humans. In: M, VL.; Beardsley, SA.; Rushton, S., editors. *Optic Flow and Beyond*. Dordrecht: Kluwer Academic Press; 2004. p. 109-137.
- Van Oostende S, Sunaert S, Van Hecke P, Marchal G, Orban GA. The kinetic occipital (KO) region in man: an fMRI study. *Cerebral Cortex*. 1997; 7:690–701. [PubMed: 9373023]
- Woods RP, Cherry SR, Mazziotta JC. Rapid Automated Algorithm for Aligning and Reslicing PET Images. *J. Comput. Assist. Tomogr*. 1992; 16:620–633. [PubMed: 1629424]
- Worsley KJ, Evans AC, Marrett S, Neelin P. A three-dimensional statistical analysis for CBF activation studies in human brain. *Journal of Cerebral Blood Flow and Metabolism*. 1992; 12:900–918. [PubMed: 1400644]
- Worsley KJ, Marrett S, Neelin P, Vandal AC, Friston KJ, Evans AC. A unified statistical approach for determining significant signals in images of cerebral activation. *Human Brain Mapping*. 1996; 4:58–73. [PubMed: 20408186]
- Yan L, Imbrosci B, Zhang W, Neubacher U, Hatt H, Eysel UT, Mittmann T. Changes in NMDA-receptor function in the first week following laser-induced lesions in rat visual cortex. *Cereb Cortex*. 2012; 22:2392–2403. [PubMed: 22089426]
- Zepeda A, Sengpiel F, Guagnelli MA, Vaca L, Arias C. Functional reorganization of visual cortex maps after ischemic lesions is accompanied by changes in expression of cytoskeletal proteins and NMDA and GABA(A) receptor subunits. *J Neurosci*. 2004; 24:1812–1821. [PubMed: 14985421]
- Zepeda A, Vaca L, Arias C, Sengpiel F. Reorganization of visual cortical maps after focal ischemic lesions. *Journal of Cerebral Blood Flow and Metabolism*. 2003; 23:811–820. [PubMed: 12843784]

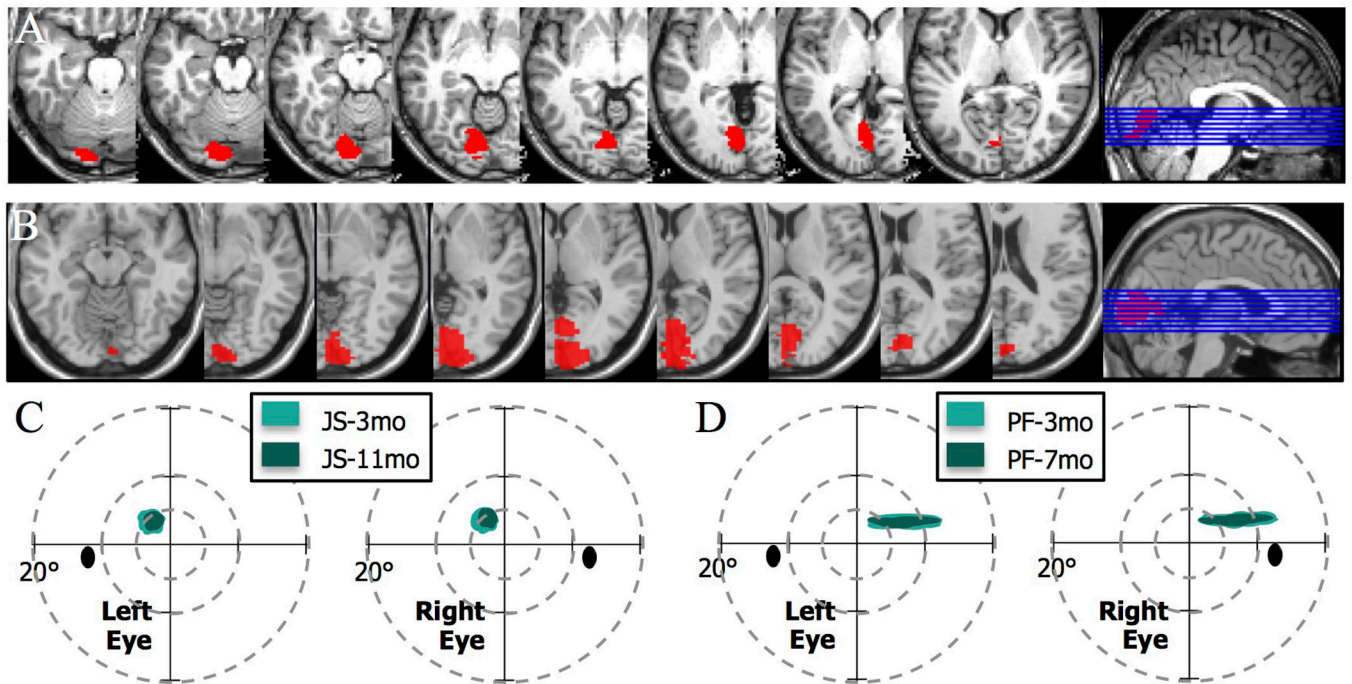


Figure 1. Lesion localization and visual field maps for patients JS and PF

(A,B) Axial slices of the T2 weighted image obtained in structural magnetic resonance scans (Siemens 3T) showing lesion locations, with a sagittal view indicating the positions of the slices, for (A) JS, and (B) PF. The right hemisphere infarction of Patient JS involved part of the primary visual cortex, and the immediately adjacent extrastriate areas. Patient's PF infarct involving part of the primary visual cortex and immediately surrounding extrastriate areas in the left occipital lobe and minimally extending in the adjacent medial temporal lobe. (C,D) Schematic of Humphrey automated perimetry for mapping visual field loss. Perimetry in patient JS was obtained at 3 months and 9.5 months after the lesion and showed a paracentral upper left scotoma, initially 5 deg in diameter with the dense part of the scotoma reduced to 3.5 deg diameter at the later assessment. The field loss corresponded to a reduction in the cortical representation of the visual field (details in Supplement 1 which illustrates a progressive recovery of the visual field representation in visual cortex at 3, 8 and 11 mo post-stroke). Perimetry of patient PF showed a stable visual field loss in the upper-right quadrant at 3 and 7 mo post-stroke.

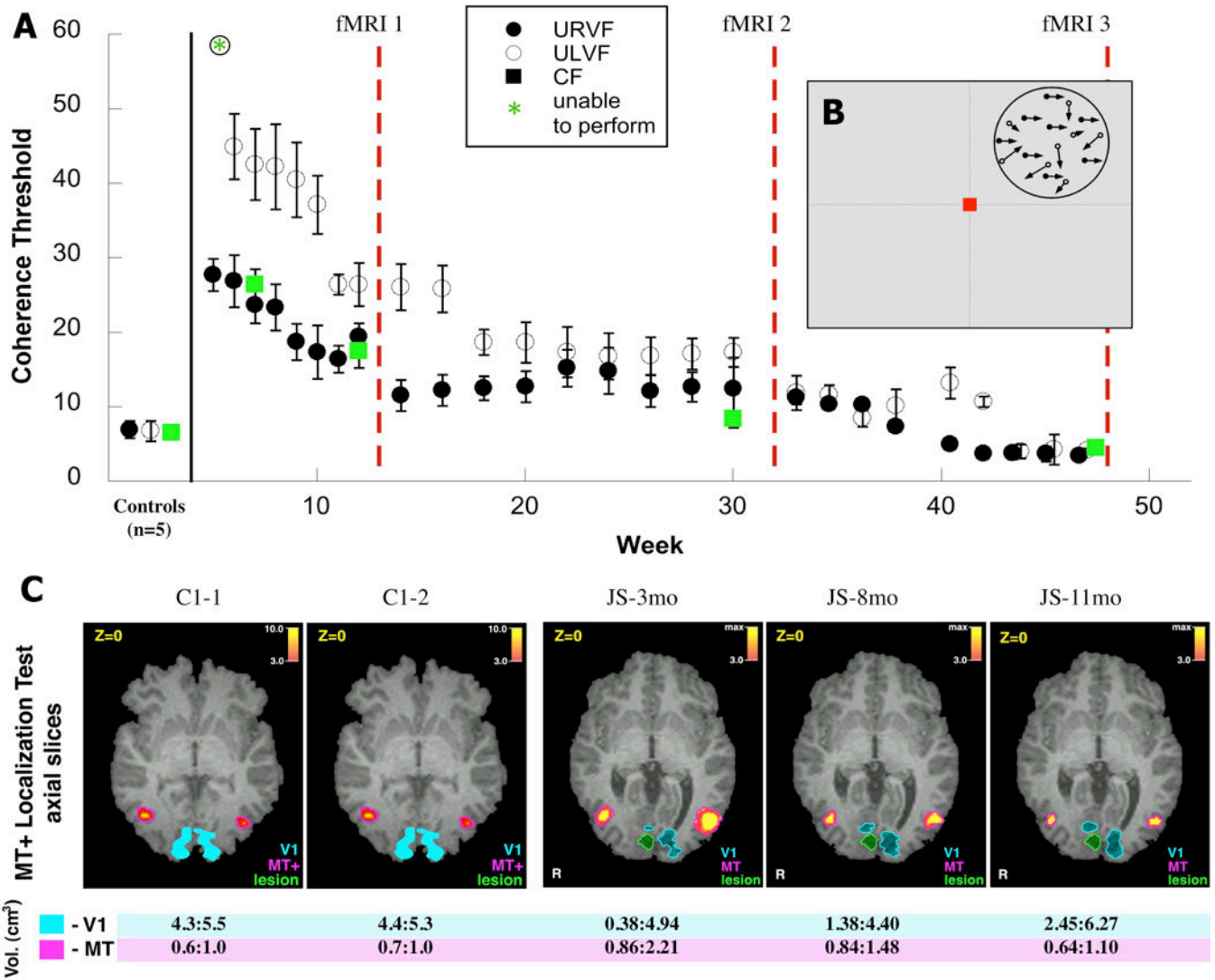


Figure 2. Learning motion coherence

(A) Performance of patient JS on the motion coherence task during training in the 11 months following his stroke. Dots show mean coherence thresholds (the proportion of signal dots necessary to perform the task) from staircases collected at the beginning of each training session \pm s.e.m. The timing of fMRI scans performed at 3, 8 and 11 mo post-stroke relative training are indicated by red dotted lines. Data is shown for both upper left (open circles), upper right (closed circles) and central visual field (green squares) testing. Data is shown for all sessions prior to the 1st fMRI scan (during which JS improved rapidly), monthly between scans 1 and 2 (when performance was relatively constant), and for all sessions between scans 2 and 3 (when performance gradually approach that of healthy controls). (B) Motion coherence stimulus. A random dot field was placed in a single quadrant of the visual field. For each pair of frames, a proportion of dots (specified by the coherence) were moved translationally (e.g., displaced left/right), while the remaining dots were repositioned randomly. (C) Comparison of the size of visual areas V1 and MT+ in a control subject C1 and patient JS in fMRI scans collected over multiple sessions (2 scans, 6mo apart for C1,

scans at 3, 8 and 11mo post-stroke for JS). (Top) fMRI activation maps in the MT+ localization test were projected on axial slices of the structural MRI image, locations of areas V1, MT+ and the lesion are shown in the corresponding colors. (Bottom) Size of activation (volume) of hMT+ in response to a central visual field motion coherence stimulus at each fMRI scan.

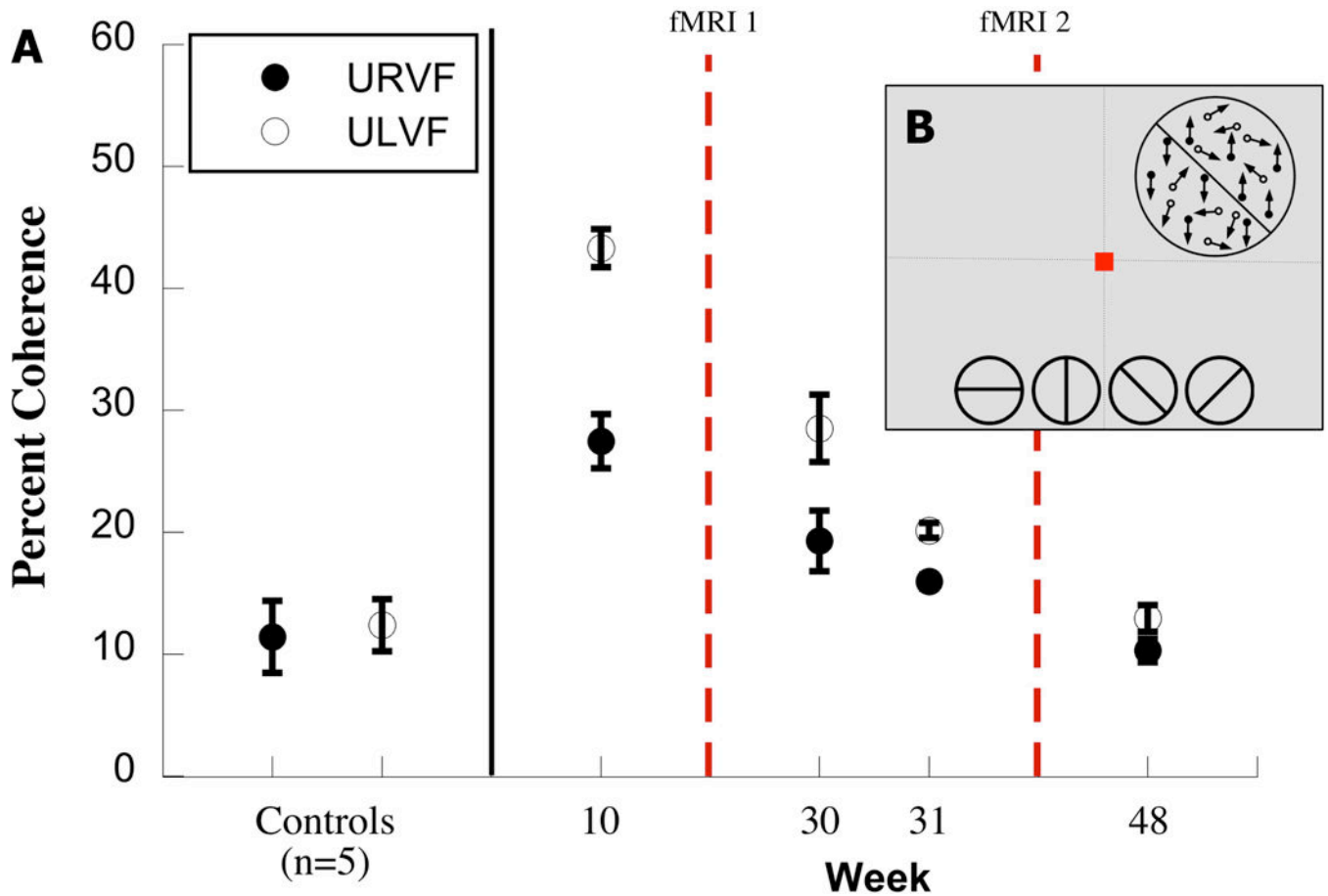


Figure 3. Motion Discontinuity (MDT)

The motion discontinuity stimulus is shown schematically. The display was either homogeneous (all signal dots moved up or down) or was divided along an illusory horizontal, vertical or diagonal boundary defined by signal dots on either side of it moving in opposite directions (up or down). In a 2AFC task, subjects had to identify whether the motion display was homogeneous (all signal dots moved in the same direction) or whether an illusory boundary traversing the middle of (shown along the bottom 2 alternative forced choice task). The stimuli, 6° in diameter were shown in the Upper left or right quadrant; 3B: The figure shows thresholds coherence on the MDT tasks in 5 healthy subjects and in JS. Patient JS took the task 4 times, a week before the first fMRI scanning at 3 months after the lesion, and then again twice in the week before the second fMRI on this task, and after the second fMRI. The Y axis, indicates the percent coherence, and the X axis, the weeks when Patient JS took the psychophysical task.

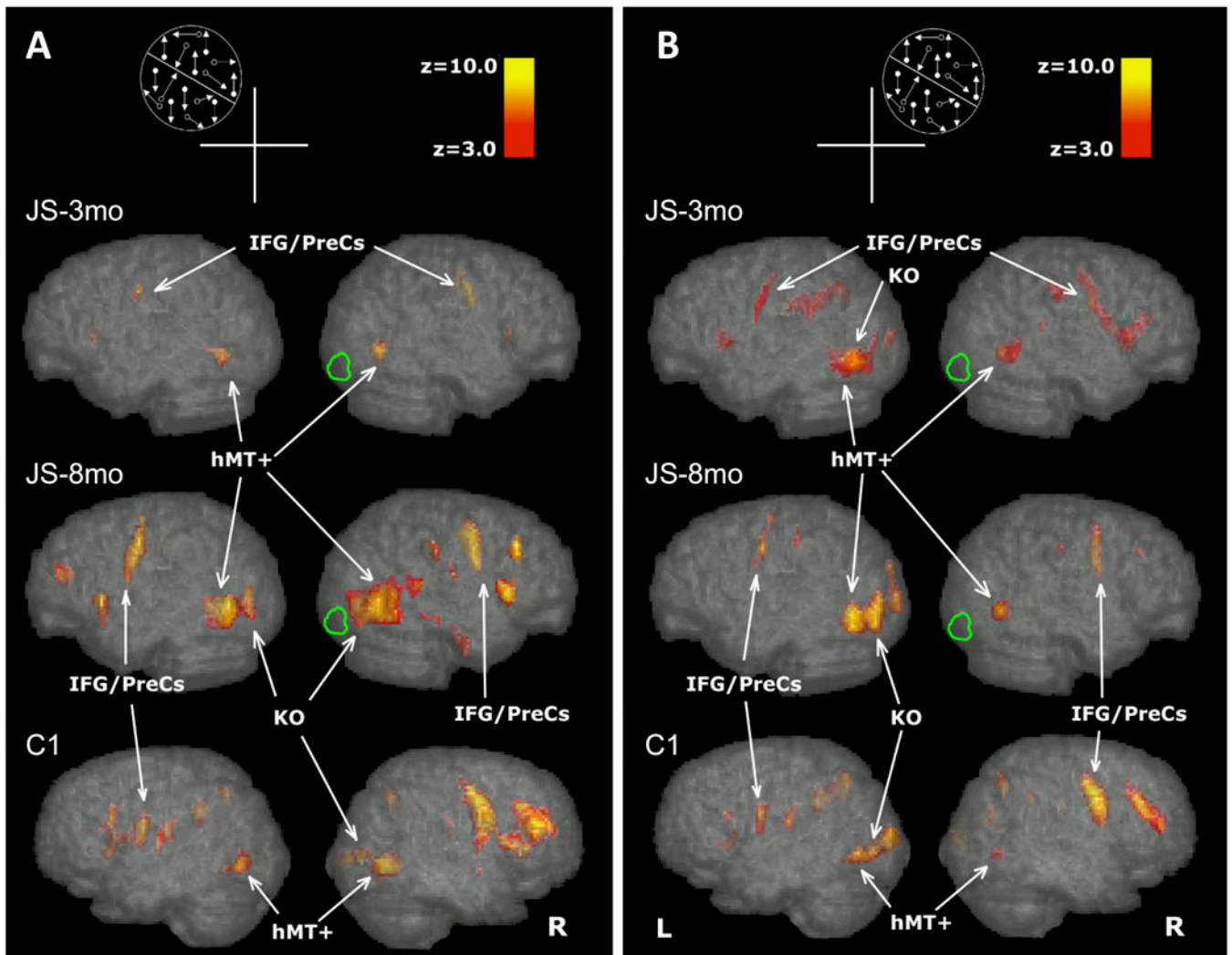


Figure 4. BOLD signal ($Z > 3$) for the Motion Discontinuity Test displayed on the MNI brain, lateral view of the right and left hemispheres of JS at 3 and 8 months after the lesion and a healthy control (C1-1). The location of the Motion Discontinuity stimulus, in the upper quadrant ipsilesional or contralesional is shown schematically in Figures 4A and 4B. The arrows, point to the activations in the areas MT+ and KO. Figure 4A shows the activations when the stimulus was shown in the upper left visual field quadrant. Fig 4B shows the activations when the stimulus was shown in the upper right visual field quadrant. MT+: middle temporal area (MT) and the middle superior temporal area (MST); KO: kinetic occipital region; IFG: inferior frontal gyrus; preCS: PreCentral Sulcus

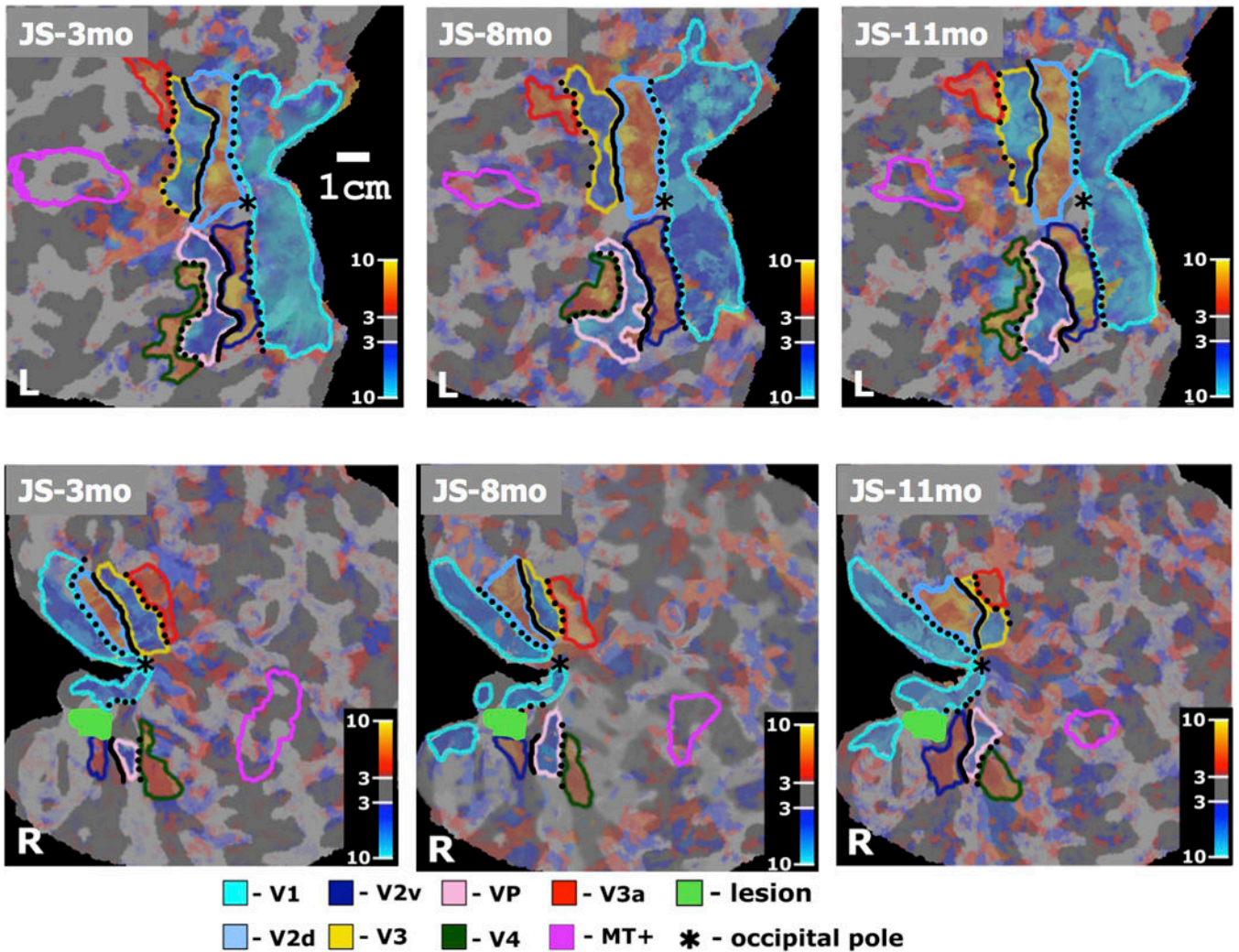


Figure 5.

Cortical representation of the tVFS maps of retinotopic visual areas V1, V2d, V2v, V3, VP, V3a, V4, and area MT+ outlined in different colors (shown in the Figure legend) and projected on the flattened representation of the cortical gray matter, separately for the left and right hemisphere. Characteristic alternation pattern of negative and positive field sign areas seen in the representation of the left hemisphere of patient JS. Abnormal retinotopy pattern is seen in the right hemisphere, in which only islands of continuity of the tVFS map representation were found. The intensities of maps are weighted by the t-statistical maps identical to the tVFS maps. Cortical representation of the vertical meridian is shown in dotted black line and representation of the horizontal meridian is shown in solid black line. (JS-3mo, L) First scan of patient JS, left hemisphere. (JS-8mo, L) Second scan of patient JS, left hemisphere. (JS-11mo, L) Third scan of patient JS, left hemisphere. (JS-3mo, R) First scan of patient JS, right hemisphere. (JS-8mo, R) Second scan of patient JS, right hemisphere. (JS-11mo, R) Third scan of patient JS, right hemisphere. The color-bar refers to the t-values of the tVFS maps (significance of the retinotopic response).

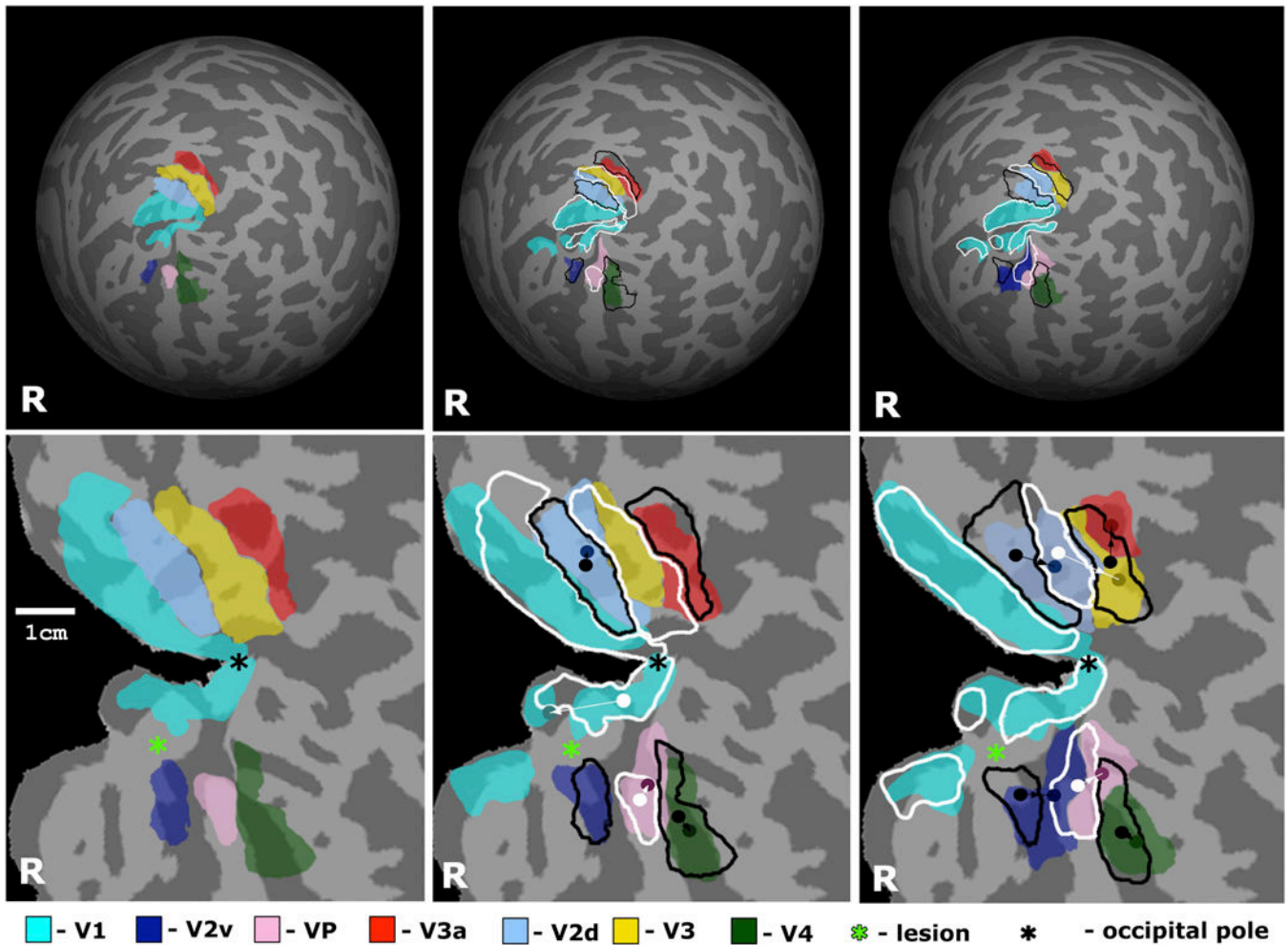


Figure 6.

Reorganization of retinotopic visual areas in the affected (right) hemisphere of patient JS shown on the reconstructed brain surface. Areas V1, V2d, V2v, V3, VP, V3a, and V4 are shown in different semi-transparent colors as specified in the Figure legend. Location and size of visual areas in the previous scan is outlined in white or black, for negative field sign and positive field sign areas respectively. (Top) Overtime changes in retinotopic visual areas registered in spherical coordinate system. Data from three scans of patient JS are shown: JS-3, 8 and 11 mo. (Bottom) Overtime changes in retinotopic visual areas overlaid on the flattened representation of the occipital cortex. Locations of the center of mass of areas V2d, V2v, V3, VP, V3a, and V4 are shown by dots having same color as specified in the Figure legend, but decreased brightness. Locations of the center of mass of the same areas in the previous scan are shown by white or black dots, for negative field sign and positive field sign areas correspondingly. Directions of reorganization of retinotopic areas V2d, V2v, V3, VP, V3a, and V4 are shown by arrows. The table shows the distance of shifts of the center of mass (in mm) estimated in spherical coordinates for the above retinotopic areas in the lesioned right hemisphere, between the first and second scan (top row) and between the

second and third scan (bottom row). The shifts in JS' normal left hemisphere and in healthy controls are shown in Table 2.

Author Manuscript

Author Manuscript

Author Manuscript

Author Manuscript

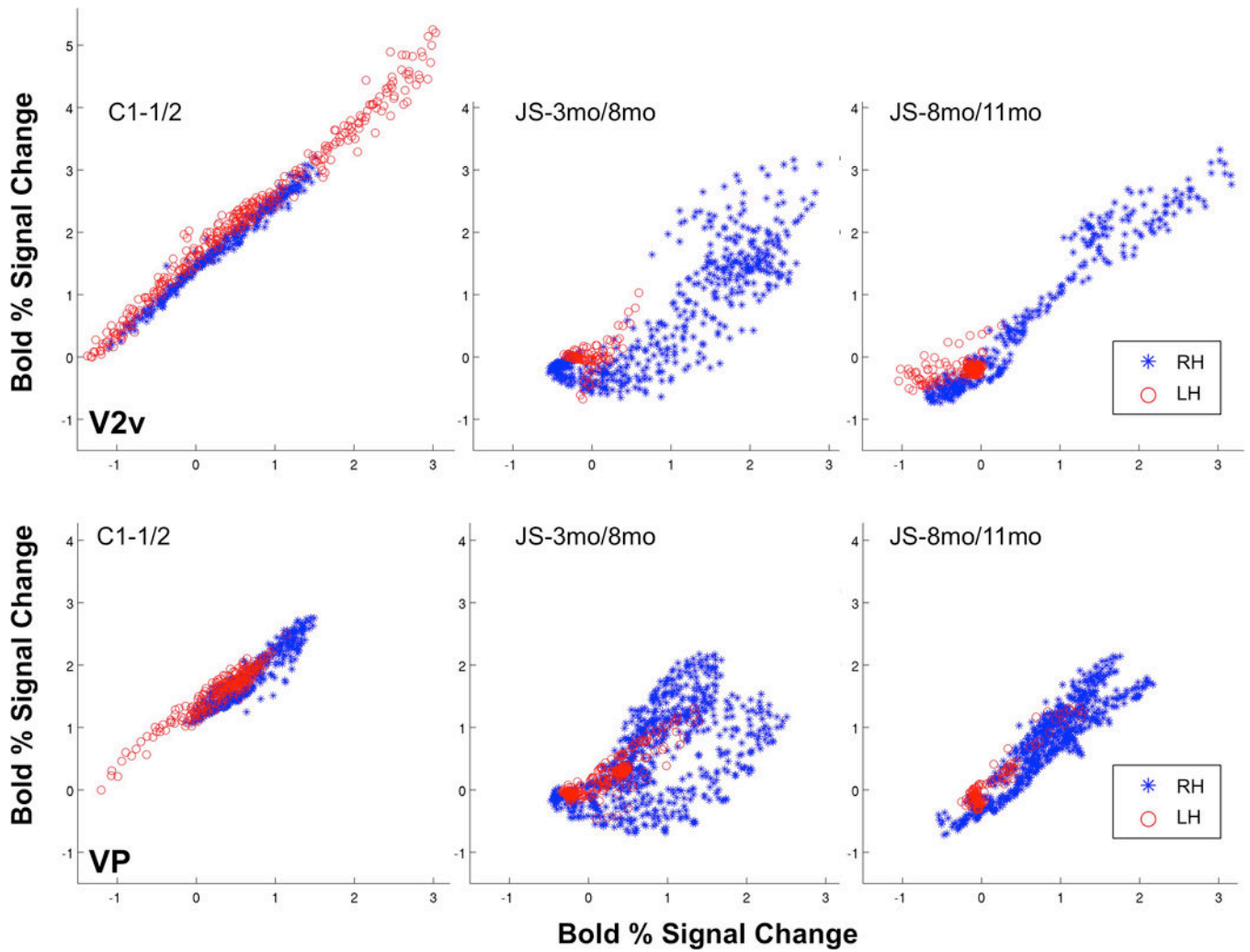


Figure 7.

Scatter plots for areas (top) V2v and (bottom) VP as defined by retinotopy mapping. X and Y-axis values indicate % BOLD signal change for voxels in the ROI at the earlier time point, for the two consecutive scans. Left hemisphere scatter plot is shown in red asterisks, right hemisphere scatter plot is shown in blue circles. Coefficients of correlation for ROI defined for both hemispheres are printed on each plot. Correlation values for areas V2v, V2d, VP and V3 in both hemispheres are given in Table 3.

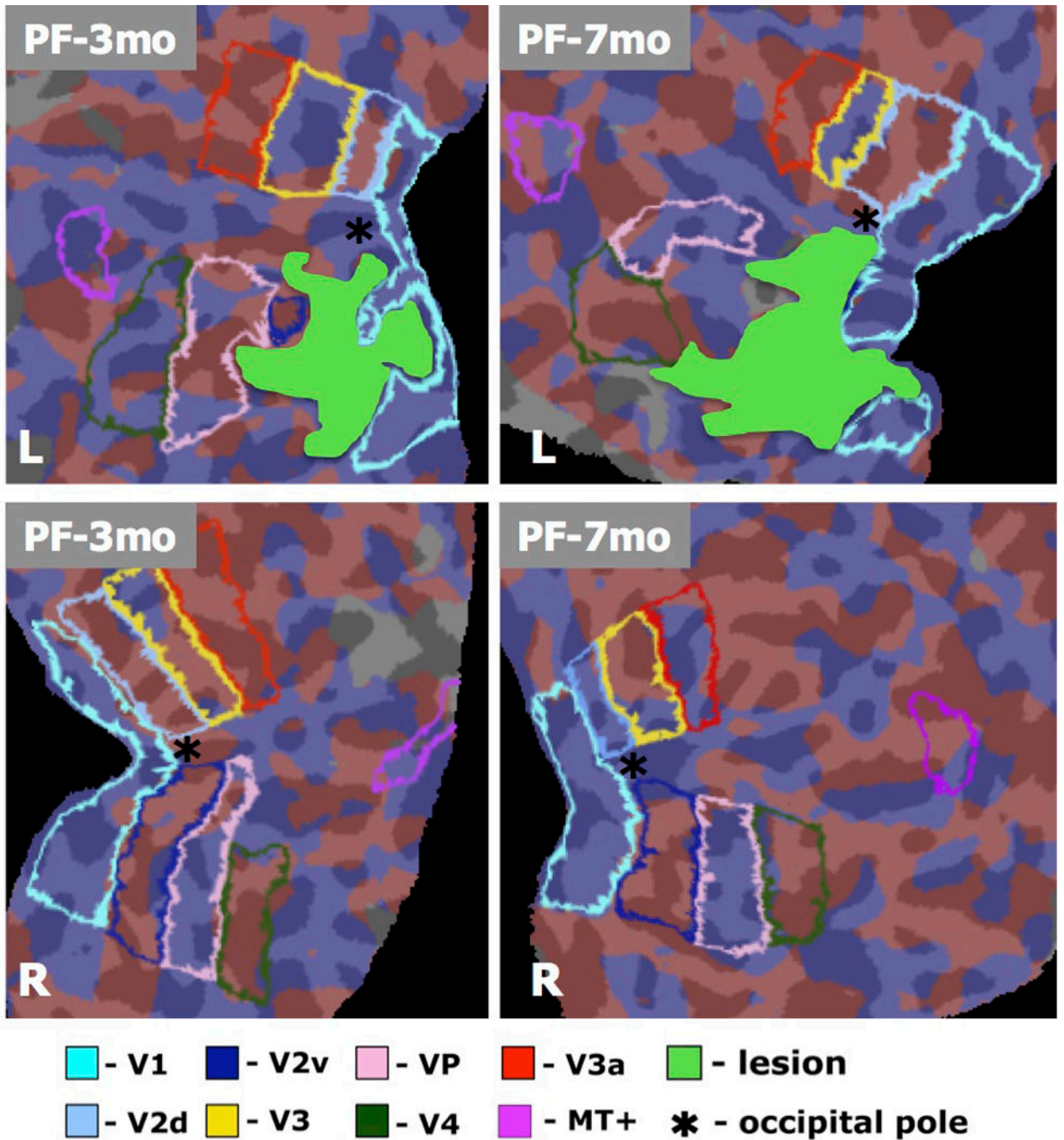


Figure 8.

Retinotopic maps for a retrospective patient study (patient PF), computed based on the standard FreeSurfer pipeline (Engel et al. 1994; Sereno et al. 1995; DeYoe et al. 1996; Engel et al. 1997)., using the same stimulus as presented to patient PF and the control. Data was acquired 3 and 7 months post-stroke, and visual areas were identified by mapping the polar and eccentricity maps to the cortical surface and identifying field sign boundaries. Borders

were identified automatically in FreeSurfer, and confirmed by manual inspection. Visual areas are shown in different colors (see Legend), with the lesion shown in solid green.

Author Manuscript

Author Manuscript

Author Manuscript

Author Manuscript

Relative ROI size between hemispheres (ratio of ipsilesional to contralesional surface area) for patients JS and PF and a healthy control (C1).

Table 1

ROI	JS I/C 0-3 mo	JS I/C 3-8 mo	JS I/C 8-11 mo	PF I/C 0-3 mo	PF I/C 0-7 mo	CI RH/LH 0 mo	CI RH/LH 0-6 mo
V1	0.37	0.48	0.52	0.88	1.71	0.78	0.83
V2v	0.19	0.17	0.52	0.08	0.08	0.95	0.92
V2d	0.58	0.59	0.74	0.62	1.66	1.28	1.29
V3v/VP	0.21	0.40	0.48	1.31	0.84	0.92	0.96
V3	0.94	0.61	0.38	1.12	0.74	1.38	1.30
V3a	1.57	1.50	0.79	0.92	0.98	0.98	1.12
V4	0.85	0.75	0.66	1.45	1.30	1.16	1.21
MT+	0.90	0.89	0.64	0.90	0.96	0.64	0.66

Shift in ROI center of mass (mm) between successive scans for patient JS and a healthy control (CI).

Table 2

ROI	JS I (RH) 3/8mo	JS I (RH) 8/11mo	JS C (LH) 3/8mo	JS C (LH) 8/11mo	CI RH 0/6mo	CI LH 0/6mo
V2v	0.8	1.7	1.5	1.5	0.0	0.2
V2d	1.5	5.2	0.8	0.8	0.0	0.5
V3v/VP	3.8	4.9	1.5	1.2	0.5	0.5
V3	0.6	6.9	0.4	0.0	0.2	0.0
V3a	1.6	4.1	1.1	1.5	0.2	0.2
V4	1.5	3.7	1.9	1.2	0.5	0.2

Normalized cross-correlation coefficients calculated between BOLD signal percent change in the full-field checkerboard stimulus (for V2v, V2d, VP and V3) and the MT localizer (for hMT+) used in the scatter plots above.

Table 3

	V2v (0/r)	V2d (0/r)	VP (0/r)	V3 (0/r)	MT+ (0/r)
CI-1 vs. CI-2	1.0/ 1.0	1.0/ 0.9	1.0/ 1.0	1.0/ 1.0	0.9/ 0.7
JS-3mo vs. JS-8mo	0.9/ 0.4	0.8/ 0.2	0.9/ 0.7	0.9/ 0.8	0.3/ 0.6
JS-8mo vs. JS-11mo	0.9/ 0.7	0.9/ 0.4	1.0/ 0.7	0.8/ 0.5	0.5/ 0.8